Received: 30 August 2022 | Revised: 8 November 2022 | Accepted: 15 November 2022

DOI: 10.1002/eqe.3783

SPECIAL ISSUE ARTICLE

WILEY

Exploring the site dependency of fragility functions in risk-targeted design

Matthew J. Fox[1] | **Gerard J. O'Reilly**[2]

[1]Department of Civil Engineering and Architecture, University of Pavia, Pavia, Italy

[2]Centre for Training and Research on Reduction of Seismic Risk (ROSE Centre), Scuola Universitaria Superiore IUSS Pavia, Pavia, Italy

Correspondence
Matthew J. Fox, Department of Civil Engineering and Architecture, University of Pavia, Via Ferrata 3, Pavia 27100, Italy.
Email: matt.fox@unipv.it

Abstract

In the ongoing quest for improved seismic design codes, there is currently substantial focus on risk-targeted design, which aims to achieve more uniform seismic risk across code-compliant buildings. Such an approach has already been adopted in ASCE 7, which uses lognormal fragility functions, with a single assumed value for dispersion, to generate uniform risk spectra. One challenge to this approach is that fragility functions have been shown to vary depending on the site being considered. This article, therefore, explores the extent to which site location influences the dispersion of fragility functions through the study of inelastic single-degree-of-freedom systems. Twenty-four different sites across New Zealand are considered so that a diverse range of seismic hazard settings, including multiple tectonic region types, are examined. The resulting dispersion values for the cases examined range from 0.14 to 0.29 and they are shown to be influenced by both the spectral shape and variance of the target spectra used for ground motion selection. The study is then extended to the consideration of scenario-based seismic risk analysis. It is shown that fragility functions derived using ground motions selected on the basis of probabilistic seismic hazard analysis are, in theory, not suitable for use in scenario-based risk analyses. The potential ramifications of this work on other risk-targeted design methods are also discussed. Overall, this work sheds important light on the importance and potential implications of site dependence for what concerns risk-targeted design.

KEYWORDS

fragility functions, risk-targeted design, scenario-based risk analysis, site dependence

1 | INTRODUCTION

Over the last couple of decades, there has been an increased focus on developing risk-targeted approaches with a view to implementing them in future revisions of seismic design codes.[1–6] The objective of such approaches is to achieve more uniform levels of seismic risk for structures designed in accordance with the minimum requirements set out by such codes. This is in contrast to the more conventional approach of designing for uniform hazard using deterministic approaches, which ultimately leads to variable levels of risk dependent on factors such as site characteristics and building typology, among others. This has been made relatively clear in a recent study in Italy described in Iervolino et al.,[7] for example,

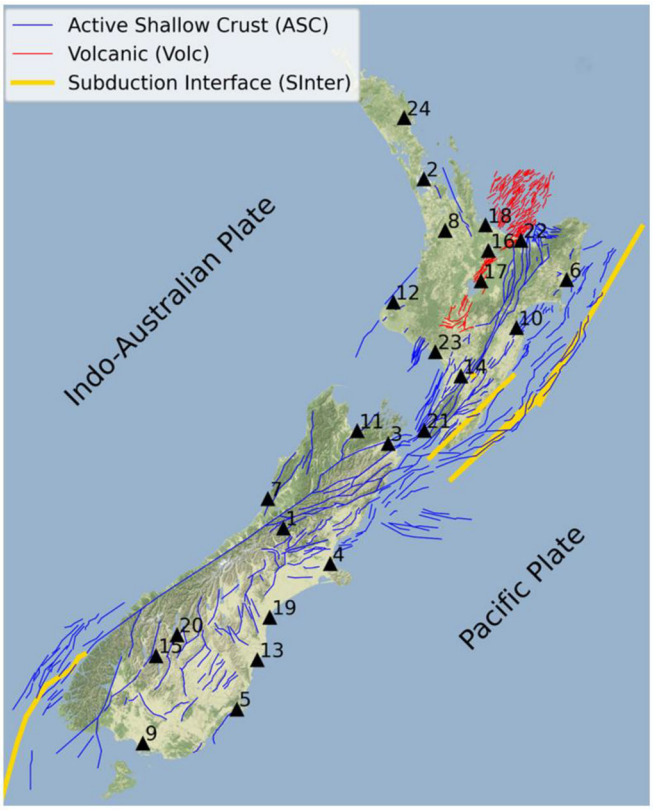

#	Site Name	Z [g]
1	Arthurs Pass	0.6
2	Auckland	0.13
3	Blenheim	0.33
4	Christchurch	0.22
5	Dunedin	0.13
6	Gisborne	0.36
7	Greymouth	0.37
8	Hamilton	0.16
9	Invercargill	0.17
10	Napier	0.38
11	Nelson	0.27
12	New Plymouth	0.18
13	Oamaru	0.13
14	Palmerston N	0.38
15	Queenstown	0.32
16	Rotorua	0.24
17	Taupō	0.28
18	Tauranga	0.20
19	Timaru	0.15
20	Wanaka	0.30
21	Wellington	0.40
22	Whakatāne	0.30
23	Whanganui	0.25
24	Whangārei	0.13

FIGURE 1 Location of the 24 sites considered in this study and corresponding seismic hazard factor, *Z*, from NZS1170.5. The mapped fault sources considered in the 2010 version of the New Zealand National Seismic Hazard Model are shown, with different colours indicating different tectonic region types. Note that for clarity the background seismicity model, which comprises a grid of points and includes subduction slab (SSlab) sources, is not shown

who demonstrated the lack of uniformity in seismic reliability amongst structures of different typologies and site hazard all designed to the same building code.

While many proposals have been made in recent years, the most well-established approach for risk-targeted design is the method proposed by Luco et al.,[1] which was implemented in ASCE 7–10[8] and subsequent editions of ASCE 7 in the United States. This approach, described in more detail in Section 2, uses a fragility curve represented by a lognormal distribution with an assumed constant value of dispersion to generate uniform risk spectra. These are then utilised as the design spectra for application in the selected code-based seismic design method. However, one challenge to such an approach is that the fragility function dispersion typically varies from site-to-site and from structure-to-structure due to both aleatory (e.g., ground motion record-to-record variability) and epistemic (e.g., numerical modelling uncertainty) uncertainties. This site-to-site variation in dispersion has been examined previously, for example, by Kohrangi et al.,[9] and is the primary focus of this article.

Given the critical nature of providing representative levels of dispersion in fragility curves utilised in risk-targeted design and the factors known to impact it, this paper explores the extent to which fragility curves are site dependent through the analysis of inelastic single-degree-of-freedom (SDOF) systems at multiple sites. New Zealand was chosen as a testbed for this study due to the considerable variation in seismic hazard across the country. As can be seen in Figure 1, the seismic hazard is driven by the plate boundary between the Pacific and Indo-Australian plates. Off the east coast of the North Island, the Pacific plate subducts beneath the Indo-Australian plate. The situation is reversed to the southwest of the country, with the Indo-Australian plate subducting beneath the Pacific plate. Between the two subduction zones is an extensive system of crustal faults, the most notable being the Alpine fault, which extends along a significant portion of the west coast of the South Island. There is also a notable volcanic area in the North Island, where earthquakes are characterised by more substantial attenuation of ground motions. The 24 sites, selected following the work of Bradley et al.,[10] correspond to major centres across New Zealand and vary significantly in terms of seismic hazard. This is evident

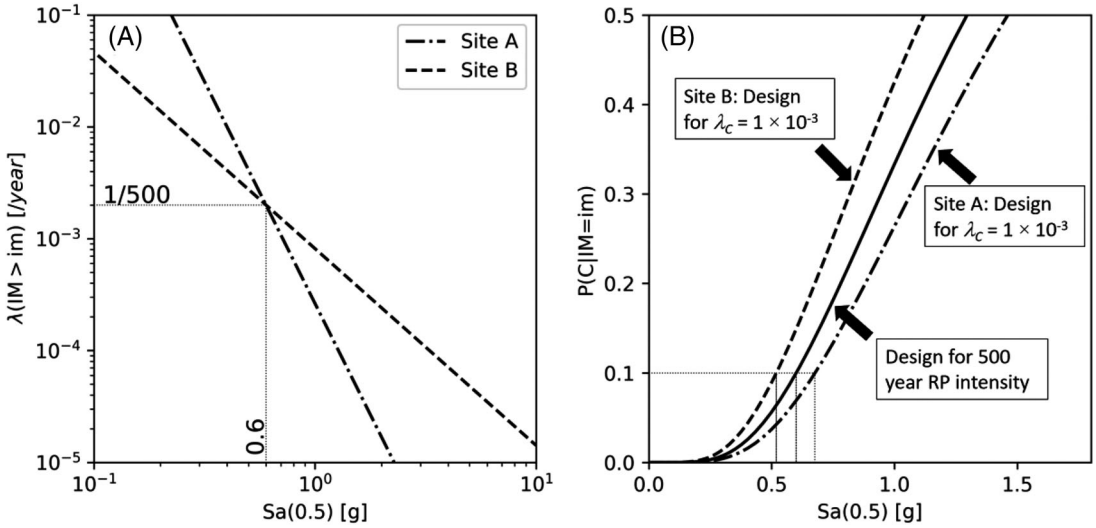

FIGURE 2 A hypothetical example of risk-targeted design: (A) hypothetical hazard curves for the two sites, which have the same intensity at the design return period of 500 years but differ in slope, and (B) fragility curves for conventional and risk-targeted design methods

from Figure 1 but also via the seismic hazard factor, Z, defined in accordance with the New Zealand seismic loading standard NZS1170.5.[11]

Section 2 of this article provides additional background on risk-targeted design and illustrates its sensitivity to certain user choices to better define the problem being tackled. The methodology adopted in the research is then explained in Section 3 before a detailed analysis and discussion of the results is performed in Section 4. Section 5 extends the work to look at the case of earthquake scenarios, and Section 6 looks at the implications of this work on other risk-targeted design methods, whereas conclusions are then provided in Section 7.

2 | BACKGROUND ON RISK-TARGETED DESIGN

As mentioned previously, the approach of Luco et al.[1] and ASCE 7 is the most well-established approach to risk-targeted design. Given its fundamental importance to the remainder of this paper, the key ideas are herein explained with reference to a hypothetical example. In this example, a building with a fundamental period of vibration of $T = 0.5$ s is designed for two different sites, Site A and Site B, for a hazard level corresponding to a return period of 500 years. As seen in Figure 2, the two sites are assumed, for the sake of example, to have the same value of $Sa(0.5) = 0.6$ g at the 500-year return period but very different hazard values at other intensities. The consequence is that following a traditional 'intensity-based' design (e.g., Eurocode 8[12] or NZS1170.5[11]), identical structural designs will result for both sites.

At this point, several issues arise in the so-called 'intensity-based' approach to seismic design when striving towards uniform risk, which has been discussed in Vamvatsikos,[13] amongst others. The first issue relates to the resulting fragility curves for the structures at Sites A and B, in tandem with the slope of the hazard curves shown in Figure 2A. If for argument's sake, the two structures were assumed to have an identical collapse fragility curve, characterised by a lognormal distribution with median, θ, and dispersion β_C, the annual rate of collapse, λ_C, computed via Equation (1), would not be equal for the simple fact that the slopes of the hazard curves at Sites A and B differ.

$$\lambda_C = \int_0^{+\infty} P\left[C|IM = im\right] \left|d\lambda\left(IM > im\right)\right| = \int_0^{+\infty} \Phi\left[\frac{\ln\left(\frac{im}{\theta}\right)}{\beta_C}\right] \left|d\lambda\left(IM > im\right)\right| \quad (1)$$

where IM refers to the intensity measure being considered, $P[C|IM = im]$ is the probability of collapse conditional on IM, $|d\lambda(IM > im)|$ is the absolute value of the derivative of the site's hazard curve and Φ is the cumulative distribution function of the standard normal distribution.

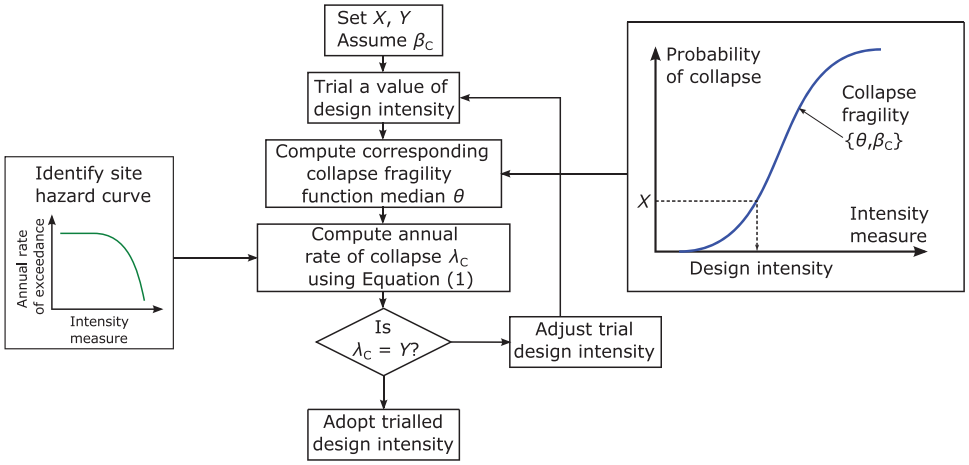

FIGURE 3 Schematic illustration of the methodology followed in risk-targeted design

Using the solid fragility curve shown in Figure 2B to represent the single collapse fragility curve for both sites' structures with the two different site hazard curves shown in Figure 2B, Equation (1) returns an annual rate of collapse of $\lambda_C = 1.79 \times 10^{-3}$ and $\lambda_C = 7.91 \times 10^{-4}$ for Site A and Site B, respectively. This is despite the 500-year return period design intensity being the same at both sites.

The problem described above via a simple example shows one of the fundamental issues of expecting uniform risk design across multiple sites of varying seismicity using an intensity-based approach. The problem is further exacerbated by the fact that structures, despite being designed to the same return period intensity as per the previous example, will generally not have the same fragility curve, as was assumed. This issue has been demonstrated by Kohrangi et al.[9] for several sites located around Turkey, where a building assessed using different ground motion sets selected via several record selection procedures produced notably varying fragility curves at the different sites. They showed that this site dependence tends to be most prominent when spectral acceleration at a known period of vibration, $Sa(T)$, is used as the *IM*. It is briefly acknowledged that this is not necessarily a critical issue always and it can be remedied via other IM definitions typically used in assessment,[9] but for code-based design it nevertheless remains problematic.

The problems described above discuss the issue from a retrospective assessment point of view, where the site hazard and structure's fragility curve are known, or are readily calculable quantities. Turning this discussion to seismic design, and more specifically risk-targeted design, the implications of some of these problems are worth exploring further. In risk-targeted design, the general approach schematically illustrated in Figure 3 is to assume that the design delivers a structure that has an X% probability of collapse at the design intensity. The next step is to assume that the collapse fragility of the structure can be represented by a lognormal distribution with a median θ and dispersion β_C. If the risk-targeted value for the annual rate of collapse, Y, is known, Equation (1) can be used to integrate the site's hazard curve and trialled collapse fragility function parameters $\{\theta, \beta_C\}$ to get the actual annual rate of collapse, λ_C. This value of λ_C is compared with the target value Y and should they differ, the median value of the collapse fragility, θ, is adjusted. The design intensity corresponding to $P[C] = X$% illustrated in Figure 3 is then used to identify the lateral forces and size the structural members for the seismic design.

As has been previously mentioned, there have been many different studies and investigations into suitable values of both X and Y. Douglas and Gkimprixis[14] give a useful overview, noting how Y can typically range from $10^{-5} - 10^{-3}$ depending on the region.[15] Other studies [e.g.,[2],[16]] looked into alternative values of X that were generally much lower than the $X = 0.10$ assumed in ASCE 7. Gkimprixis et al.[17] provided a useful nomogram to illustrate the interaction between these assumed values and other parameters needed to implement risk-targeted design. One of the parameters listed in Figure 3 is the assumption of β_C, which is set at a fixed value of $\beta_C = 0.6$ in ASCE 7, although Luco et al.[1] initially suggested 0.8. Gkimprixis et al.[17] demonstrated how the assumed value of dispersion had a notable impact on the resulting design intensity following Figure 3.

Applying the risk-targeted approach of ASCE 7 to the hypothetical example and targeting an annual rate of collapse of $\lambda_C = 1 \times 10^{-3}$, the fragility curve must be shifted to the right for Site A and to the left for Site B (Figure 2B). The resulting design intensities are then 0.67 g and 0.52 g for Site A and Site B, respectively. The process illustrated in Figure 3 can also be applied to investigate the impact of the likely scenario of different structures having different values of β_C. Considering

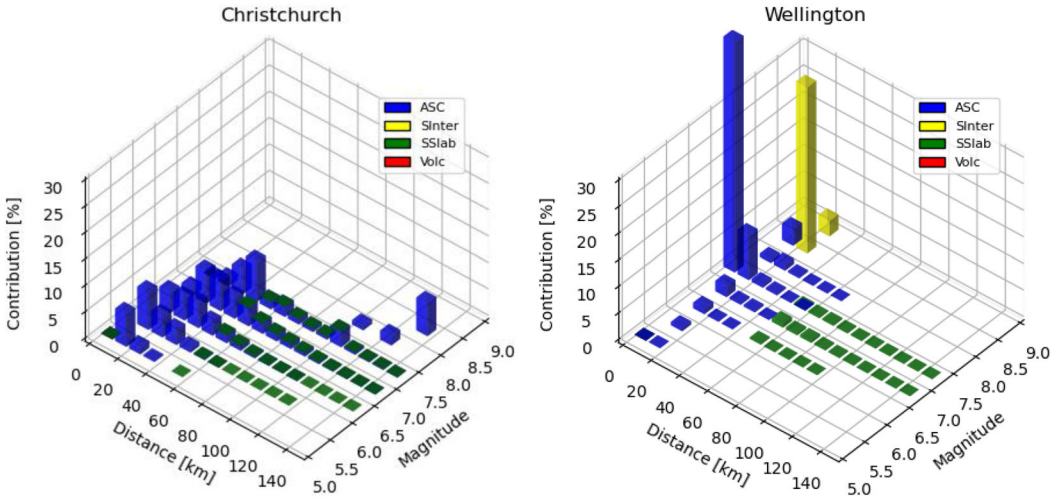

FIGURE 4 Seismic hazard disaggregation in terms of magnitude, distance and TRT for Christchurch and Wellington for the IML3 intensity

only Site A, the same annual rate of collapse of $\lambda_C = 1 \times 10^{-3}$ is targeted, but two different dispersion values of $\beta_C = 0.4$ and $\beta_C = 0.8$ are assumed. For $\beta_C = 0.4$ the resulting design intensity reduces to 0.59 g whereas for $\beta_C = 0.8$ it increases to 0.91 g. Clearly, the choice of β plays a significant role when targeting uniform seismic risk.

3 | METHODOLOGY

3.1 | Seismic hazard analysis

Probabilistic seismic hazard analysis (PSHA) was performed for the 24 sites illustrated in Figure 1 using the OpenQuake Engine v3.11[18] and the seismic source model of Stirling et al.[19] Ground-motion models (GMMs) were selected for each of the four different tectonic region types (TRTs) in the source model. For Active Shallow Crust (ASC) and Volcanic TRTs, the GMM of Bradley[20] was used because it is the most recent New Zealand-specific GMM. For subduction interface and subduction slab TRTs, the model of Abrahamson et al.[21] was adopted. All sites were assumed to have an average shear-wave velocity in the top 30 m of soil of $V_{S,30} = 300$ m/s, and for use in the Bradley[20] GMM, the $Z_{1.0}$ parameter was assumed to be 459 m.

For each site, the seismic hazard in terms of $Sa(0.5)$ was calculated for a return period of 500 years (i.e., $Sa(0.5)_{500}$), using the geometric mean definition of spectral acceleration.[22] Seismic hazard disaggregation was then performed, using the occurrence approach,[23,24] for four different intensities, IML1[1] to IML4, corresponding to 0.75, 1.0, 1.25, and 1.5 times $Sa(0.5)_{500}$, respectively. In addition to the standard approach of disaggregation in terms of magnitude and distance, the TRT was also included. This was considered necessary for the subsequent step of ground-motion selection, and as can be seen in Figure 4, the contributions from different TRTs can vary substantially between sites. For the case of Christchurch, there are contributions from a wide range of magnitude and distance pairs, and the hazard mostly comes from ASC sources, with a small contribution from subduction slab (SSlab) sources. The hazard in Wellington, on the other hand, is dominated by events on either the nearby Wellington Fault (ASC) or the Hikurangi subduction zone (SInter).

3.2 | Ground-motion selection

To carry out dynamic analysis on different SDOF systems, 25 ground motions were selected for each site and intensity. The Generalised Conditional Intensity Measure (GCIM) and the corresponding selection algorithm described in Bradley[25]

[1] Here the terms 'intensity' and 'intensity measure level' are used interchangeable, with the latter being abbreviated as IML. This is to distinguish it from 'intensity measure' or IM, which refers to a specific type of intensity measure, e.g., *PGA* or *Sa*(T1)

TABLE 1 Additional parameters for use in ground-motion selection

TRT	GMM	Additional GMM parameters			
		Dip	Rake	Z_{tor}	Backarc
Active Shallow Crust (ASC)	Bradley[20]	90°	0°	0	–
Volcanic (Volc)	Bradley[20]	90°	0°	0	–
Subduction Interface (Sinter)	Abrahamson et al.[21]	–	–	–	No
Subduction Slab (SSlab)	Abrahamson et al.[21]	–	–	–	No

were used for the selection of ground motions. However, the conditioning intensity measure (IM) was $Sa(0.5)$ and the vector of conditional *IM*s comprised only spectral accelerations, so in this sense the approach was very similar to the conditional spectrum approach.[26,27] The reader is referred to Bradley[25] for a full description of ground-motion selection using the GCIM method and herein only the key steps are reported:

1. For the selected site and intensity, a random rupture (rup_i) was obtained from the disaggregation probability mass function (rather than using the mean or mode, for example). In this case, the rupture was defined in terms of magnitude, M, closest distance to the rupture plane, R and TRT, and the other rupture parameters (e.g., hypocentral depth, rake angle) were judiciously selected based on common properties of similar fault sources within the seismic source model (see Table 1).
2. For rup_i, the conditional multivariate (normal) distribution of ground-motion intensity measures was calculated. In this case, the ground-motion intensity measures comprised spectral accelerations at 64 different periods logarithmically spaced between 0.1 and 4 s, inclusive. The actual calculation was performed as per Jayaram et al.,[9] using the specific GMM corresponding to the TRT being considered (see Table 1) and correlation coefficients from the equations in Baker and Jayaram.[28]
3. For each rup_i, a correlated vector of conditional intensity measures was stochastically generated from the multivariate distribution.
4. Ground motions were drawn from an appropriate database and scaled to match the simulated intensity measure vector (in this case a simulated response spectrum) by minimising the sum-of-squared-errors (SSE), as per Equation (2). The ground motion with the lowest SSE was then selected.

$$SSE = \sum_{j=1}^{N} (\ln Sa(T_j) - \ln Sa^{(s)}(T_j))^2 \tag{2}$$

   where $Sa(T_j)$ is the spectral acceleration of the scaled ground motions at the period T_j, $Sa^{(s)}(T_j)$ has the same meaning, but for the simulated response spectrum, and N is the number of periods being considered.
5. Steps 1 to 4 were repeated for $n_{GM} = 25$ ground motions. This number was chosen on the basis that it is at the upper end of what might be used in practice, and initial trials with a larger number created problems due to the limited number of suitable ground motions not requiring excessive scaling,[29] which was particularly evident for subduction events.
6. Typically, once the set of n_{GM} ground motions is selected, an overall residual can be calculated for the set, based on its fit to the target conditional distributions. As noted in Bradley,[25] this is important for when n_{GM} is small and less so for larger ground motions sets. As a relatively large number of ground motions was used in this study, the check of the goodness of fit of the set was limited to a visual check of the selected spectra against the target.

Two ground-motion databases were used for the selection process. In the cases of rup_i corresponding to ASC or volcanic TRTs, ground motions were selected from the NGA-West2 database,[30] and for subduction events, ground motions were selected from a preliminary set of 500 ground motions from the NGA-Sub database.[31] To be considered for selection, ground motions from these databases had to meet the additional criteria reported in Table 2. It is noted that slightly looser criteria were used for subduction interface events, due to the limited size of the available database.

Figure 5 shows the response spectra of the selected ground motions for both the Christchurch and Wellington sites at the IML3 intensity. Visual comparison of the median and 16th/84th percentile spectra for the target and selected motions shows a reasonably good fit in both cases. In the case of Wellington, the spectra corresponding to 10 ground motions from

TABLE 2 Constraints on candidate ground motions, where M* and R* indicate the target magnitude and distance, respectively

Constraint	Allowable value(s)
Magnitude	$M^* \pm 1$
Site-to-source distance	$0.5R^*$ - $2R^*$
Site-to-source distance (Sinter)	$0.33R^*$ - $3R^*$
$V_{S,30}$ [m/s]	100–600
Scale factor	0.33–3
Scale factor (Sinter)	0.25–4
Max # ground motions from single event	7

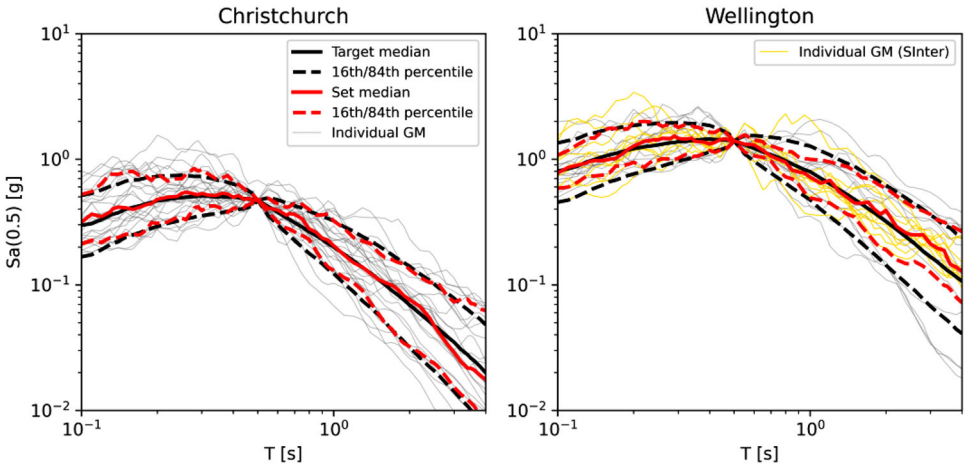

FIGURE 5 Target spectra and response spectra of selected motions for Christchurch and Wellington for the IML3 intensity. The 10 subduction interface motions for Wellington have been indicated in the plot

subduction interface events are highlighted. Note that because they all come from the same rupture scenario, they tend to be grouped closely together. This also shows how ground motions from different TRTs can be used in the collective conditional selection of ground motion records.

The aforementioned ground-motion selection process inevitably led to individual ground motions being selected multiple times for different sites and different intensities. The highest level of repetition for a single ground-motion record was 26 times across 12 different sites (but always with a different scaling factor), after which the level of repetition reduced rapidly for other ground motions. This could potentially lead to a reduction in the site-to-site variability; however, given the large total number of ground motions, the impact is expected to be minor.

3.3 | Structural analysis

To obtain structural response data for fragility analysis, multiple stripe analysis (MSA)[32] was performed on 24 inelastic SDOF systems, one for each site. The SDOFs had a period of vibration of $T = 0.5$ s and were designed via traditional intensity-based design with a force reduction factor of $R = 2$ at the 500-year return period intensity. In other words, the yield strength of each SDOF was set as per Equation (3):

$$F_y = \frac{Sa(0.5)_{500}m}{R} \tag{3}$$

where m is the mass of the system.

Non-linear time-history analysis of the SDOFs was performed using Ruaumoko3D[33] with Newmark constant average acceleration numerical integration and a timestep of 0.005 s. A bilinear hysteresis rule was used, with the post-yield stiffness set at 5% of the initial stiffness. The damping model employed for the analyses was tangent stiffness proportional, with

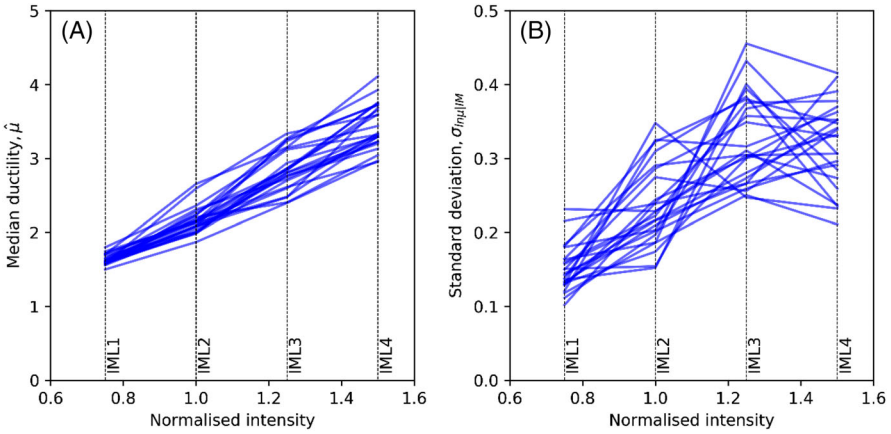

FIGURE 6 MSA results expressed in terms of (A) median ductility and (B) logarithmic standard deviation

the damping ratio set at 5% of critical. It is important to note that up to this point all references to spectral acceleration have been to the geometric mean of the two as-recorded horizontal components of the ground motion. For structural analysis, the two as-recorded components were applied separately and the maximum ductility from either of the two analyses was taken as the engineering demand parameter (EDP) of interest. This is conceptually similar to the 3D structural analysis of a building with two identical, independent, orthogonal lateral load-resisting systems. While it is acknowledged that there may be different approaches on how to address such an issue,[22] since the scope of this work is to investigate the relative difference in dispersions across different sites, and the magnitude of their potential impact in risk-targeted design, this decision was not anticipated to have any significant impact on the findings of this work.

Figure 6 illustrates the MSA results for all sites and SDOFs in terms of the median ductility demand, $\hat{\mu}$, and logarithmic standard deviation of the ductility demand at each IML examined, $\sigma_{\ln\mu|\mathrm{IM}}$. These IMLs have been normalised to the reference return period of 500 years (i.e., IML2) as previously mentioned. As expected, there is a reasonable level of site-to-site variation in the median ductility demands, due to the variation in seismic sources impacting each site. Furthermore, it is noted that site-to-site trends tend to be consistent across IMLs, i.e., a specific site tends to consistently produce stronger (or weaker) ductility demands at all four IMLs. From Figure 6B it can be observed that the standard deviation increases with intensity due to the increasingly non-linear behaviour in the SDOF systems. It is important to note though that the total standard deviation is not solely due to inelastic behaviour but is also a consequence of how spectral acceleration has been defined (i.e., in terms of geometric mean of two components). This means that even at low intensities (i.e., in the elastic range) there is uncertainty in the structural response.

3.4 | Fragility analysis

Following the structural analysis, a ductility of $\mu_{\mathrm{lim}} = 2.5$ was chosen to represent an arbitrary limit state. The maximum likelihood method, as described by Baker[34] and Iervolino,[35] was then used to fit a lognormal fragility function to the analysis data. Figure 7 shows the fragility curves for all 24 sites and corresponding SDOF systems. It is clear from Figure 7A that there is a significant range in terms of median values, θ, owing to the significant variations in seismic hazard across the 24 selected sites. However, in addition to the differences in the median, it can also be seen that there is a large variation in dispersion in Figure 7B when a visual comparison is carried out via the normalisation of each fragility curve by its median value.

4 | RESULTS

4.1 | Dispersion values for 24 sites

Figure 8 shows the dispersion values of the fragility functions obtained for each site. It can be seen that there is a reasonable level of variation between them, despite the SDOFs being essentially identical (other than F_y, which was set in

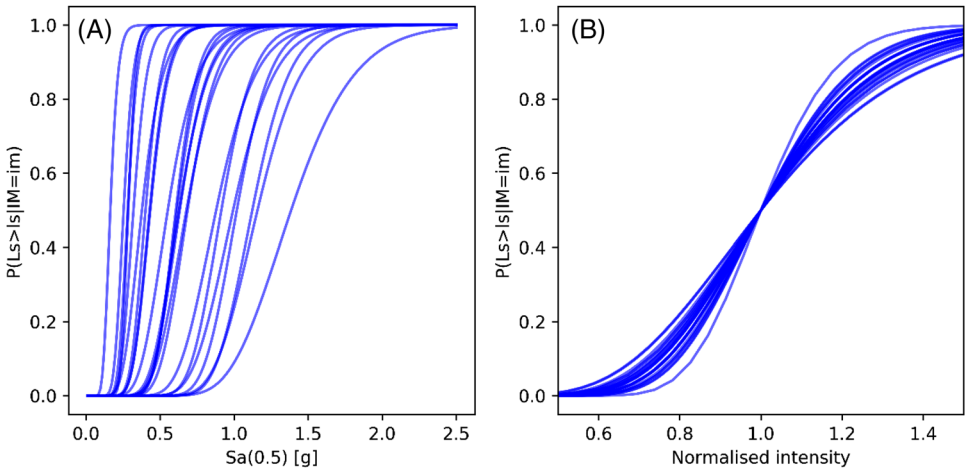

FIGURE 7 (A) Fitted lognormal fragility functions (B) fragility functions normalised by their median value and exhibiting variation in dispersion, β

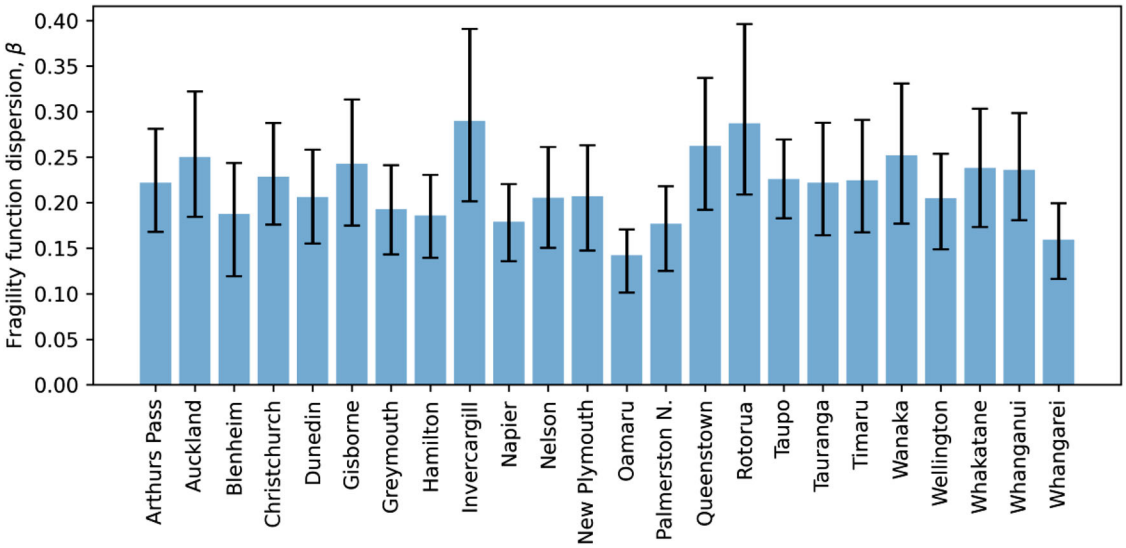

FIGURE 8 Fragility function dispersion, β, for 24 sites and the corresponding 90% confidence intervals

proportion to $Sa(0.5)_{500}$), with values ranging between 0.14 for Oamaru and 0.29 for Invercargill. It is underlined here that the dispersion values shown in Figure 8 consider only record-to-record variability and do not incorporate other sources of uncertainty such as model parameter type uncertainty, for example.

Important in such an analysis is the consideration of epistemic uncertainty in the estimates of β, in particular owing to the limited number of analyses at each intensity. To obtain a measure of the epistemic uncertainty, bootstrap resampling[36] was used to simulate sets of 1000 fragility curves for each site and associated SDOF system and subsequently estimates of the 90% confidence interval (CI) about the estimated value of β, which are illustrated via the whiskers shown in Figure 8.

In lieu of a more formal statistical treatment of epistemic uncertainty, the 90% CI bounds in Figure 8 were used to evaluate whether the differences in dispersion could be treated as statistically significant. It is clear that across all sites there is significant uncertainty in the estimates of dispersion due to record-to-record variability. Whilst the uncertainty could be reduced by increasing n_{GM}, it is not necessarily feasible in all cases due to the limited number of ground motions in the databases used (in particular for subduction zone events) and also the issues of excessive ground motion scaling that would be required to find a sufficiently large set of suitable ground motions. Furthermore, for typical analysis of structures at a design practice level, the number of analyses (100 in total) would already be considered computationally demanding in most cases. Notwithstanding the large uncertainty, it can be seen that for certain combinations of sites (e.g., Oamaru and Invercargill) the difference could likely be considered as statistically significant, meaning that the differences

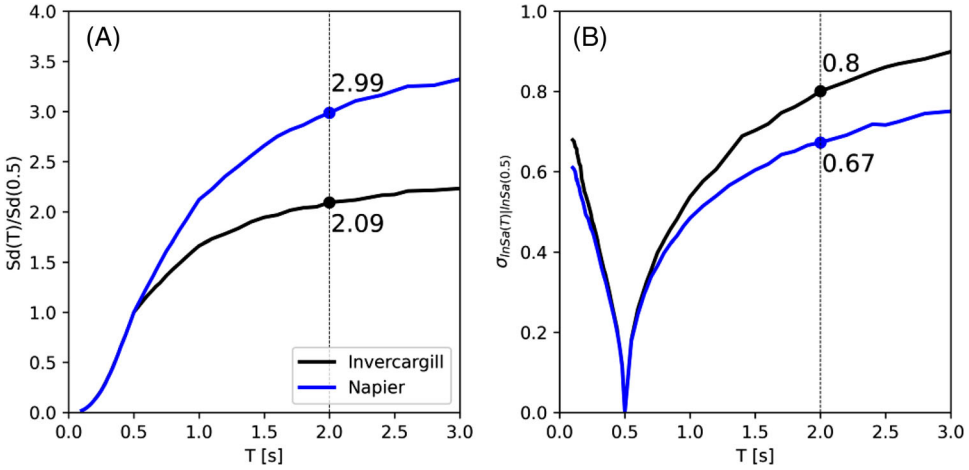

FIGURE 9 Illustration of ad hoc proxies used for ground motion spectral shape and variance: (A) ratio of median spectral displacements at periods T and 0.5 s. (B) conditional standard deviations of the target spectra. Both plots are for IML4

can be taken as due to the differences in seismic source characteristics, including from different TRTs, and subsequently the ground motion records used to represent them.

4.2 | Analysis of factors influencing dispersion

Further analysis of the results from Figure 8 is herein used to provide some insight into factors potentially influencing the dispersion at each site. Giving first some consideration to the factors that can affect fragility function dispersion, there are two: (i) the central tendency (i.e., mean) of the analysis results at each intensity, and (ii) the spread (i.e., variance) of the analysis results at each intensity. For what concerns the central tendency, it should be considered that due to the difference in site-to-site characteristics, the properties of the selected records will have some influence on the average ductility demand, as was noted in Figure 6A, for example. Past research[37–39] has indicated that for simple inelastic SDOF systems (without strength degradation), the most influential factor is spectral shape. In terms of constraining the fit of fragility functions, spectral shape is most important at the higher intensities where inelastic response of the SDOF systems is more pronounced and the spectral shape of conditionally selected ground motions would tend to be quite 'peaked' (i.e., as opposed to 'valleyed[37]').

To investigate further, ratios of spectral displacements, $Sd(T)$, were used as an ad hoc proxy for spectral shape. Specifically, the ratio of $Sd(2)/Sd(0.5)$ for IML4 was considered. This is illustrated in Figure 9A, where ratios of 2.09 and 2.99 are obtained for reference sites of Invercargill and Napier, respectively.

This spectral shape proxy was then plotted for all sites along with the corresponding β value in Figure 10A. It can be observed that there is a weak trend for β to decrease as the $Sd(2)/Sd(0.5)_{IML4}$ ratio increases. This is logical as the higher $Sd(2)/Sd(0.5)_{IML4}$ ratio tends to elicit a larger displacement response and increases the conditional probability of exceeding the limit state ductility at IML4. This in turn has the effect of steepening the fragility curve.

A similar process was used to investigate the effect of conditional variance in the target ground motion spectra on the fragility function dispersion. The conditional standard deviation of the IML4 target spectrum at a period of $T = 2$ s (i.e., $\sigma_{\ln Sa(2)|\ln Sa(0.5)}$) was used as a proxy for conditional variance in the target spectrum. This is illustrated for the Invercargill and Napier reference sites in Figure 9B, where values of 0.8 and 0.67, respectively, are obtained. Plotting this proxy against β in Figure 10B shows that as the conditional variance of the selected ground motions increases, so too does dispersion in the fragility curves.

As well as investigating the characteristics of the ground motion sets that led to differences in β, the underlying seismological characteristics of each site were investigated. Figure 11A shows β against $Sa(0.5)_{500}$ for each site, which indicates that there is no apparent trend in dispersion as a function of the seismic hazard level at the reference return period. On the other hand, Figure 11B shows that there is some relationship between β and the contribution from different TRTs. This is represented via the parameter *%ASC*, which refers to the percentage of hazard from ASC sources and is obtained from

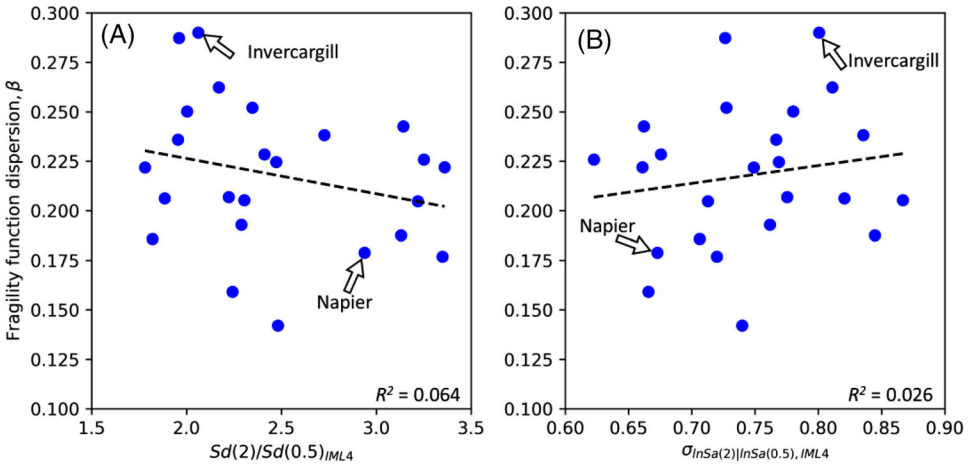

FIGURE 10 Fragility function dispersion plotted against: (A) spectral displacement ratio, $Sd(2)/Sd(0.5)$, and (B) standard deviation of the target spectrum at $T = 2$ s, $\sigma_{\ln Sa(2)|\ln Sa(0.5)}$. In both cases corresponding to IML4

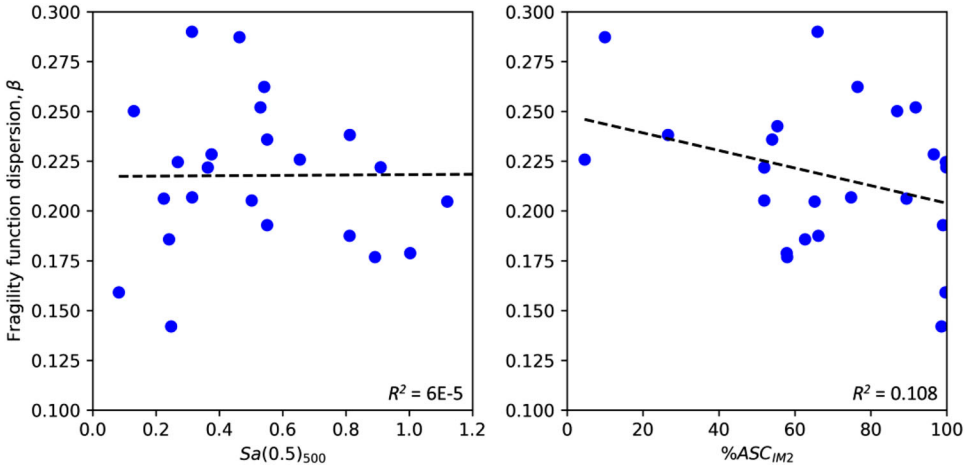

FIGURE 11 Fragility function dispersion plotted against: (A) seismic hazard in terms of $Sa(0.5)_{500}$, and (B) percentage contribution of ASC sources at IML2

disaggregation as per Equation (4) (adapted from[51]):

$$\%ASC = 100\% \times \sum_{rup_i \in ASC} \frac{P(IM = im|rup_i)\lambda(rup_i)}{\lambda(IM = im)} \tag{4}$$

where $rup_i \in$ ASC denotes a fault rupture that belongs to the set of ASC ruptures.

As the percentage of hazard from ASC sources decreases (and essentially gets replaced by a mix of the other three seismic sources) there tends to be an increase in dispersion. This could be explained as being a result of the increased contributions from multiple TRTs, each associated with a different GMM (Table 1), which in turn increase the variance in the target response spectrum and subsequently the fragility function dispersion.

5 | EXTENSION TO SCENARIO-BASED RISK ANALYSIS

Following the results presented in the previous section, consideration can also be given to what implications these findings have when seismic risk analyses are performed considering scenario-based hazard. Scenario-based hazard refers to the ground shaking that is expected to be observed from a single earthquake scenario (i.e., a specific fault rupture of known

magnitude M and distance R). Considering earthquake scenarios allows various stakeholders (e.g., local government, insurance providers, and owners of distributed infrastructure) to understand what the impacts of a single major event are likely to be.

For scenario-based risk analysis, it is common to represent structures using generic fragility curves that have been derived using ground motions selected on the basis of PSHA results. However, as shown in Section 4 and observed in other past studies, fragility functions are site dependent and are influenced by the multiple different earthquake rupture scenarios contributing to the hazard at a particular intensity. On the other hand, when considering scenario-based risk analysis, the analyst is only interested in what happens to the structure when it is subjected to a single scenario. This could be equated to removing all earthquake sources except for the specific rupture scenario of interest; thus, the problem is analogous to comparing different sites affected by different sources, as was done in Section 4. The corollary is that fragility functions derived using ground motions selected on the basis of PSHA results are, in theory, not suitable for use in scenario-based risk analysis.

To investigate this issue further, fragility curves were derived for six different sites and earthquake scenarios:

1. M_W 8.1 earthquake on the Alpine Fault impacting the site at Arthur's Pass;
2. M_W 6.7 earthquake on the Wairoa fault impacting the Auckland site;
3. M_W 7.1 earthquake on the Greendale Fault impacting the Christchurch site (which was the scenario experienced during the 2010 Darfield Earthquake);
4. M_W 7.4 earthquake on the Awatere fault impacting the Dunedin site;
5. M_W 7.2 earthquake on the Gable End fault affecting the Gisborne site; and
6. M_W 7.5 earthquake on the Wellington Fault impacting the Wellington site.

To derive the fragility curves, the same methodology described in Section 3 was again employed. The only difference was in the ground motion selection procedure, rather than randomly sampling ruptures from the seismic hazard disaggregation (step 1), all rup_i were instead set to correspond to the specific scenarios of interest from the list above.

Figure 12 shows the median and dispersion for the fragility curves derived previously in Section 3, which are referred to as time-based as they come from a PSHA-oriented approach, and again using ground motions selected for each specific scenario listed above, referred to as scenario-based. Substantial differences are observed in both the median and dispersion values for the Arthur's Pass, Gisborne and Wellington cases, whereas the differences are much more modest for Auckland, Christchurch and Dunedin. Given that the comparisons are analogous to the site-to-site comparisons undertaken in Section 4, the differences can again be attributed to: (i) a reduction in the conditional standard deviation of spectral accelerations when scenario-based hazard is considered due to fewer sources contributing to the ground motion record selection, and (ii) differences in spectral shape. Based on the limited data, it is not possible to identify a clear and consistent trend. However, it is clear that the most significant changes in fragility are for the higher hazard sites, each of which is dominated by events from a very small number of large-magnitude fault sources at high intensities.

It should be noted that the derivation of fragility curves for individual scenarios, as has been carried out in this section, is generally impractical for scenario-based risk analysis. This is because scenario-based risk analysis will generally need to consider a portfolio of geographically distributed structures, and the analyst may also want to consider more than one scenario. It would therefore be necessary to calculate a very large number of fragility curves (equal to the number of structures times the number of scenarios to be considered).

6 | IMPLICATIONS FOR OTHER RISK-TARGETED DESIGN PROCEDURES

Examining the results and discussions presented in previous sections, it is clear that the site-to-site variability plays a key role in a structure's collapse fragility curve, or the curve of some other critical limit state focused on in design. It was seen in Figure 8 that the record-to-record variability alone could vary between values of $\beta = 0.14$–0.29 depending on the site being considered in New Zealand. This is also in line with past work by Kohrangi et al.[9] who made a similar observation for different sites in Turkey. With this observation in mind, a brief commentary is provided here with regard to what this may mean for other risk-targeted design methods currently proposed in the literature and used in practice.

With reference to the most developed method utilised in ASCE 7, it is clear that a 'one-size-fits-all' dispersion value is not appropriate for all structures and sites and future work should investigate cases like the one presented here, but for more SDOF types with different force reduction factors. It is recalled that the results presented here were for systems with

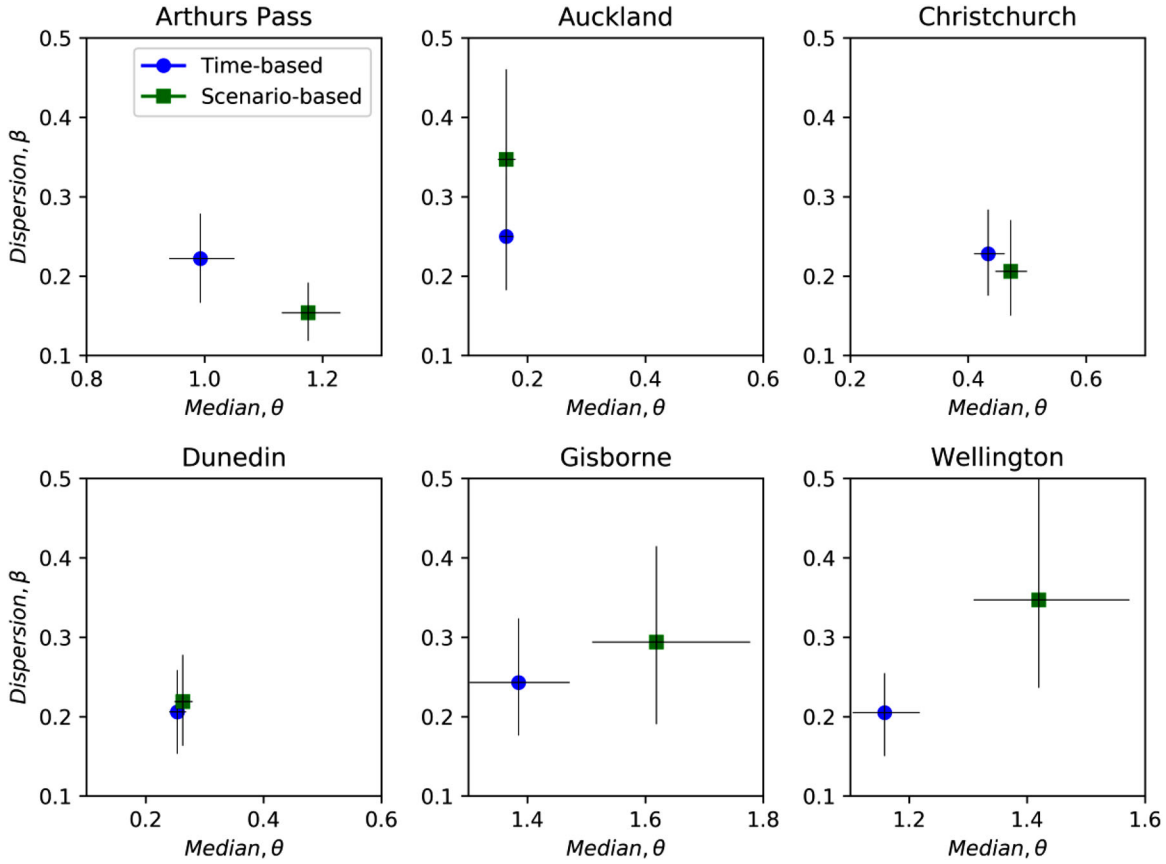

FIGURE 12 Fragility function medians, θ, and dispersions, β, for each of the six sites considering both scenario-based and time-based approaches. Error bars indicate the 90% CI

$T = 0.5$ s designed with an $R = 2$ and examined at a ductility of $\mu = 2.5$. Many more combinations of these parameters could be investigated to give more informed and practical guidance on how to treat this issue in practice.

Design methods that rely in some way on readily available R-μ-T relationships to essentially provide the link between elastic and expected inelastic response would be affected by the findings outlined here. These include traditional design and assessment methods like the N2 method[40] employed in Eurocode 8, or the SPO2IDA tool[41] employed in the FEMA P-58 guidelines[42] (which also forms the basis for design methods such as the yield frequency spectrum method[6] or the integrated performance-based seismic design method[43]). Each of these methods relies on precalculated R-μ-T relationships that were derived using a predetermined set of ground motion records. As soon as the site characteristics during the application of these methods notably differ from the distribution of ground motions used in their developments, the consistency will begin to break down slightly. The same is also true of a recent risk-targeted method to design friction pendulum isolators[44] or to the extension of the SPO2IDA tool to infilled frame systems.[45] While the above statements may appear to be rather critical, it is noted that these principally apply to methods that are based around using $Sa(T)$ as the IM. It is recalled that the work by Kohrangi et al.[9] did highlight the site-dependence issue of fragility functions but noted that the issue could be mitigated if the IM was changed to average spectral acceleration[46,47] and the ground motion record selection procedure slightly modified. Hence, remedies are available, but given the prominence of $Sa(T)$ as an IM in design, its limitations are worth highlighting nonetheless.

Other risk-targeted methods discussed in Shahnazaryan and O'Reilly[5] include the risk-targeted seismic action (RTSA) method by Žižmond and Dolšek[4] and the risk-targeted behaviour factor (RTBF) method initially outlined in Cornell.[48] One of the steps in the RTSA involves conducting an incremental dynamic analysis (IDA)[49] on a simple SDOF system to estimate the expected nonlinear demands. So long as the ground motion records used in this IDA take some consideration of the specific site characteristics of the site, the issues raised in this paper should be somewhat alleviated. Similarly, in the RTBF approach, if the process used to develop such factors gives due consideration to the site characteristics, the impacts of the work presented here should be expected to be minimal, although this does not discount other limiting aspects of the RTBF approach discussed by Baltzopoulos et al.,[50] for instance.

Nevertheless, from the above discussion it is clear that the site-dependency of fragility functions is an issue that ought not to be discounted. Its impact on different risk-targeted methods has been seen to vary depending on the approach being followed, but in all cases, it is clearly not an unsurmountable issue.

7 | CONCLUSIONS AND RECOMMENDATIONS

This work has highlighted the site dependence of fragility functions, in particular their dispersion, β, through the study of inelastic single-degree-of-freedom systems at 24 locations across New Zealand. Although there was significant epistemic uncertainty in the β estimates due to practical limitations on the number of ground motions used in the analyses, it was still shown that the differences between some sites could be considered statistically significant. Values of β ranged between 0.14 and 0.29 and it was shown that this variation was, to some extent, related to the variance in spectral accelerations of the selected ground motions and differences in spectral shape of the target spectra. It was furthermore shown that dispersion was not influenced by the level of seismic hazard at a given site but was influenced by differences in the percentage contributions from different tectonic region types.

The implication for risk-targeted design approaches like that of Luco et al.[1] and ASCE 7 is that the assumed value of dispersion should vary from site to site, and is generally the case for other recent risk-targeted design approaches. However, it is acknowledged that once the dispersion values obtained in this work are inflated by other sources of uncertainty (e.g., model uncertainty) the site-to-site variation is likely to be less pronounced. Furthermore, although derivation of site (and structure) specific fragility curves is possible, it does represent a significant increase in engineering effort. With these two points in mind, a practical recommendation would be for risk-targeted seismic design codes to utilise a limited number of different dispersion values for representing different geographical regions within the code's jurisdiction. An alternative way forward would be to develop adjustment factors that could 'correct' the dispersion values based on specific site characteristics (such as the relative contribution from different tectonic region types); however, significantly more data beyond the case study systems analysed here would need to be generated for such a purpose.

It has also been shown in this work that the use of fragility curves derived using ground motions selected on the basis of PSHA are, in theory, not suitable for use in scenario-based risk analysis. However, from the limited results, it was not possible to identify a distinct trend in the differences between so called time-based and scenario-based fragility curves. As the derivation of fragility curves for specific scenarios is highly impractical, it is recommended that further research be undertaken to develop guidance on the use of time-based fragility curves in scenario risk analyses.

ACKNOWLEDGEMENTS

The authors would like to thank Volkan Özsaraç for his assistance with the EzGM Python scripts used for ground-motion selection. Comments on this manuscript provided by Prof. Iunio Iervolino and two anonymous reviewers are greatly appreciated.

DATA AVAILABILITY STATEMENT

The author has provided the required Data Availability Statement, and if applicable, included functional and accurate links to said data therein.

ORCID

Matthew J. Fox https://orcid.org/0000-0002-5099-9532
Gerard J. O'Reilly https://orcid.org/0000-0001-5497-030X

REFERENCES

1. Luco N, Ellingwood BR, Hamburger RO, Hooper JD, Kimball JK, Kircher CA. Risk-targeted versus current seismic design maps for the conterminous United States. *Proceedings of the 2007 SEAOC convention*. California, 2007.
2. Silva V, Crowley H, Bazzurro P. Exploring risk-targeted hazard maps for Europe. *Earthquake Spectra*. 2019;32(2):1165-1186.
3. Horspool N, Gerstenberger MC, Elwood KJ, Risk targeted hazard spectra for seismic design in New Zealand. *Proceedings of the 2021 New Zealand Society for Earthquake Engineering Annual Conference*. Christchurch, 2021.
4. Žižmond J, Dolšek M. Formulation of risk-targeted seismic action for the force-based seismic design of structures. *Earthq Eng Struct Dyn.* 2019;48(12):1406-1428.

5. Shahnazaryan D, O'Reilly GJ. Integrating expected loss and collapse risk in performance-based seismic design of structures. *Bull Earthquake Eng*. 2021;19(2):987-1025.
6. Vamvatsikos D, Aschheim MA. Performance-based seismic design via yield frequency spectra. *Earthq Eng Struct Dyn*. 2016;45(11):1759-1778.
7. Iervolino I, Spillatura A, Bazzurro P. Seismic reliability of code-conforming Italian buildings. *J Earthquake Eng*. 2018;22(sup2):5-27.
8. ASCE. *Minimum Design Loads and Associated Criteria for Buildings and Other Structures (ASCE/SEI 7–10)*. Structural Engineering Institute, American Society of Civil Engineering, Reston, Virginia, 2010.
9. Kohrangi M, Vamvasikos D, Bazzurro P. Site dependence and record selection schemes for building fragility and regional loss assessment. *Earthq Eng Struct Dyn*. 2017;46:1625-1643.
10. Bradley BA, Cubrinovski M, Wentz F. Probabilistic seismic hazard analysis of peak ground acceleration for major regional New Zealand locations. *Bull NZ Soc Earthq Eng*. 2022;55(1):15-24.
11. Standards New Zealand. *NZS1170.5: Structural Design Actions. Part 5: Earthquake Actions - New Zealand*. 2004.
12. CEN. *Eurocode 8: Design of Structures for Earthquake Resistance – Part 1: General Rules, Seismic Actions and Rules for Buildings (EN 1998-1:2004)*. 2004.
13. Vamvatsikos D. *Performance-Based Seismic Design in Real Life: The Good, The Bad and The Ugly*. ANIDIS; 2017.
14. Douglas J, Gkimprixis A. Risk targeting in seismic design codes: the state of the art, outstanding issues and possible paths forward. *Seismic Hazard and Risk Assessment*. Springer Natural Hazards. Springer; 2018.
15. Braverman JI, Xu J, Ellingwood BR, Costantino CJ, Morante RJ, Hofmayer CH. *Evaluation of the seismic design criteria in ASCE/SEI standard 43-05 for application to nuclear power plants*. U.S. Nuclear Regulatory Commission Office of Nuclear Regulatory Research, Washington, DC 20555-0001, 2007.
16. Douglas J, Ulrich T, Negulescu C. Risk-targeted seismic design maps for mainland France. *Adv Clim Changes, Global Warming, Biol Probl Nat Hazards, 3rd WSEAS Int Conf Clim Changes, Global Warming, Biol Probl (CGB '10) 3rd WSEAS Int Conf Nat Hazards (NAHA '10)*. 2013;65(3):1999-2013.
17. Gkimprixis A, Tubaldi E, Douglas J. Comparison of methods to develop risk-targeted seismic design maps. *Bull Earthquake Eng*. 2019;17(7):3727-3752.
18. Pagani M, Monelli D, Weatherill G, et al. OpenQuake Engine: an open hazard (and risk) software for the Global Earthquake Model. *Seismol Res Lett*. 2014;85(3):692-702.
19. Stirling M, McVerry G, Gerstenberger M, et al. National seismic hazard model for New Zealand: 2010 update. *Bull Seismol Soc Am*. 2012;102(4):1514-1542.
20. Bradley BA. A New Zealand-specific pseudospectral acceleration ground-motion prediction equation for active shallow crustal earthquakes based on foreign models. *Bull Seismol Soc Am*. 2013;103(3):1801-1822.
21. Abrahamson N, Gregor N, Addo K. BC Hydro ground motion prediction equations for subduction earthquakes. *Earthquake Spectra*. 2016;32(1):23-44.
22. Baker JW, Cornell CA. Which spectral acceleration are you using? *Earthquake Spectra*. 2006;22(2):293-312.
23. Fox MJ. Considerations on seismic hazard disaggregation in terms of occurrence or exceedance in New Zealand. *Bull NZ Soc Earthq Eng*. in press.
24. Cito P, Iervolino I. On occurrence disaggregation of probabilistic seismic hazard. *Earthq Eng Struct Dyn*. 2022;51(14):3296-3303.
25. Bradley BA. A ground motion selection algorithm based on the generalized conditional intensity measure approach. *Soil Dyn Earthquake Eng*. 2012;40:48-61.
26. Baker JW. Conditional mean spectrum: tool for ground motion selection. *J Struct Eng*. 2011;137(3):322-331.
27. Jayaram N, Lin T, Baker JW. A computationally efficient ground-motion selection algorithm for matching a target response spectrum mean and variance. *Earthquake Spectra*. 2011;27(3):797-815.
28. Baker JW, Jayaram N. Correlation of spectral acceleration values from NGA ground motion models. *Earthquake Spectra*. 2008;24(1):299-317.
29. Dávalos H, Miranda E. Evaluation of bias on the probability of collapse from amplitude scaling using spectral-shape-matched records. *Earthq Eng Struct Dyn*. 2019;48(8):970-986.
30. Ancheta TD, Darragh RB, Donahue JL, et al. NGA-West2 database. *Earthquake Spectra*. 2014; 30(3): 989-1005.
31. Kishida T, Victor C, Yousef B, et al. NGA-Sub ground motion database. *Proceedings of the 11thNational Conference in Earthquake Engineering*, Earthquake Engineering Research Institute, Los Angeles, 2018.
32. Jalayer F, Cornell CA. Alternative non-linear demand estimation methods for probability-based seismic assessments. *Earthq Eng Struct Dyn*. 2009;38(8):951-972.
33. Carr AJ. *Ruaumoko Manual—Volume 3: User manual for the 3-dimensional version Ruaumoko3D*. Department of Civil Engineering, University of Canterbury; 2012.
34. Baker JW. Efficient analytical fragility function fitting using dynamic structural analysis. *Earthquake Spectra*. 2015;31(1):579-599.
35. Iervolino I. Assessing uncertainty in estimation of seismic response for PBEE. *Earthq Eng Struct Dyn*. 2017;46(10):1711-1723.
36. Efron B, Tibshirani R. *An Introduction to the Bootstrap*. Chapman and Hall; 1993.
37. Baker JW, Cornell CA. Spectral shape, epsilon and record selection. *Earthq Eng Struct Dyn*. 2006;35(9):1077-1095.
38. Baker JW, Cornell CA. A vector-valued ground motion intensity measure consisting of spectral acceleration and epsilon. *Earthq Eng Struct Dyn*. 2005;34(10):1193-1217.
39. Eads L, Miranda E, Lignos D. Spectral shape metrics and structural collapse potential. *Earthq Eng Struct Dyn*. 2016;45(10):1643-1659.
40. Fajfar P. A nonlinear analysis method for performance-based seismic design. *Earthquake Spectra*. 2000;16(3):573-592.

41. Vamvatsikos D, Cornell CA. Direct estimation of the seismic demand and capacity of MDOF systems through Incremental Dynamic Analysis of an SDOF approximation. *J Struct Eng*. 2005;131(4):589-599.
42. FEMA. *Seismic Performance Assessment of Buildings,FEMAP-58-1*. Prepared by the Applied Technology Council for the Federal Emergency Management Agency, 2018.
43. Shahnazaryan D, O'Reilly GJ, Monteiro R. On the seismic loss estimation of integrated performance-based designed buildings. *Earthq Eng Struct Dyn*. 2022;51(8):1794-1818.
44. O'Reilly GJ, Yasumoto H, Suzuki Y, Calvi GM, Nakashima M. Risk-based seismic design of base-isolated structures with single surface friction sliders. *Earthq Eng Struct Dyn*. 2022;51(10):2378-2398.
45. Nafeh AMB, O'Reilly GJ, Monteiro R. Simplified seismic assessment of infilled RC frame structures. *Bull Earthquake Eng.* 2020;18(4):1579-1611.
46. Eads L, Miranda E, Lignos DG. Average spectral acceleration as an intensity measure for collapse risk assessment. *Earthq Eng Struct Dyn*. 2015;44(12):2057-2073.
47. Kohrangi M, Bazzurro P, Vamvatsikos D, Spillatura A. Conditional spectrum-based ground motion record selection using average spectral acceleration. *Earthq Eng Struct Dyn*. 2017;46(10):1667-1685.
48. Cornell CA, Calculating building seismic performance reliability: a basis for multi-level design norms. *Proceedings of the 11th World Conference on Earthquake Engineering*, Acapulco, Mexico, 1996.
49. Vamvatsikos D, Cornell CA. Incremental dynamic analysis. *Earthq Eng Struct Dyn*. 2002;31(3):491-514.
50. Baltzopoulos G, Grella A, Iervolino I. Seismic reliability implied by behavior-factor-based design. *Earthquake Eng Struct Dyn*. 2021;50:4076-4096.
51. Baker JW, Bradley BA, Stafford PJ. Seismic Hazard and Risk Analysis. Cambridge University Press, 2021.

How to cite this article: Fox MJ, O'Reilly GJ. Exploring the site dependency of fragility functions in risk-targeted design. *Earthquake Engng Struct Dyn*. 2022;1-16. https://doi.org/10.1002/eqe.3783